www.sciencemag.org/content/350/6259/423/suppl/DC1

Supplementary Material for

Asteroseismology can reveal strong internal magnetic fields in red giant stars

Jim Fuller,* Matteo Cantiello,* Dennis Stello, Rafael A. Garcia, Lars Bildsten

*Corresponding author. E-mail: jfuller@caltech.edu (J.F.); matteo@kitp.ucsb.edu (M.C.)

Published 23 October 2015, *Science* **350**, 423 (2015)
DOI: 10.1126/science.aac6933

This PDF file includes:

S1 Supplementary Text

S1.1 Stellar Models

We have used the Modules for Experiments in Stellar Evolution (MESA, release 7385) code (*23, 24*) to evolve low-mass stars with initial mass in the range 1-3.0 $M_\odot$. Models have been evolved from the pre-main-sequence to the tip of the red giant branch. We chose a metallicity of $Z = 0.02$ with a mixture taken from (*25*); the plasma opacity is determined using the OPAL opacity tables from (*26*). Convective regions are calculated using the mixing-length theory (MLT) with $\alpha_{\rm MLT} = 2.0$. The boundaries of convective regions are determined using the Ledoux criterion. Overshooting is parameterized by an exponentially decaying diffusivity that decays over a distance $f_{\rm ov}H$ above the convective boundary (*27*), with $f_{\rm ov} = 0.018$. We include in Section S1.10 the inlist used for running the calculations.

To estimate plausible magnetic field strengths within the cores of red giants, we consider two scenarios: one based on observational evidence of surface fields, and one based on MHD modeling of magnetic fields in convective stellar cores. First, we extrapolate inward from a main sequence surface field of $B \sim 3\,{\rm kG}$, as appropriate for magnetic Ap stars (*20*), assuming the field is a pure dipole such that the field strength scales as $B \propto r^{-3}$. Since the radius of the convective core is typically $r_c \sim R/10$ for low mass main sequence stars, field strengths of $B > 10^5\,{\rm G}$ are attainable near the core.

Second, we estimate field strengths produced by a magnetic dynamo that operates within the convective core of a star while it is on the main sequence. In this case, MHD simulations suggest equipartition (and even super-equipartition) magnetic field strengths may be generated (*28*), i.e., magnetic fields whose energy density is comparable to that of the kinetic energy of convective flows such that

$$\frac{B^2}{8\pi} \sim \rho v_{\rm con}^2\,. \tag{S1}$$

We calculate typical core convective velocities $v_{\rm con}$ using mixing length theory. In our stellar models, we evaluate Eqn. S1 to find that core magnetic fields of $B \sim 3{\times}10^5$ G could be generated during the main sequence.

To extrapolate to field strengths plausibly obtained within the radiative cores of red giants, we assume that the magnetic flux (calculated via the methods above) within the core is conserved as it contracts. This is a good approximation for stable magnetic equilibria discussed here because the timescale for the field to diffuse through the star (the Ohmic timescale) is longer than the main sequence timescale. At each mass shell within a red giant, the field strength is then approximated by

$$B_{\rm RG} = \left(\frac{r_{\rm MS}}{r_{\rm RG}}\right)^2 B_{\rm MS}\,, \tag{S2}$$

where $B_{\rm RG}$ is the field strength while on the RGB, $r_{\rm RG}$ and $r_{\rm MS}$ are the radial coordinates of the shell on the RGB and MS, respectively, and $B_{\rm MS}$ is the MS field strength. Mass shells enclosing $M \sim 0.2\,M_\odot$ (which are located just outside the MS core and near the H-burning shell on the lower RGB) typically contract by a factor of a few from the MS to the lower RGB. The magnetic field may therefore be amplified and field strengths in excess of 10^6 G are quite plausible within the H-burning shells of RGB stars.

Fig. S1 shows the density, mass, and magnetic field profiles of the $1.6\,M_\odot$ stellar model used to generate Fig. 3. To make this model, we extrapolate a dipole field inward from a surface value of 3×10^3 G (as described above), with an artificial cap at a field strength of 5×10^4 G. We then calculate the corresponding RGB field profile using the flux conservation described above (for simplicity we set the field equal to zero in convective regions of the RGB model). This relatively conservative approach yields a field strength of $\sim 10^6$ G at the H-burning shell, sufficient for magnetic suppression of dipole oscillation modes. We note that field strengths of this magnitude are orders of magnitude below equipartition with the gas pressure, and therefore have a negligible influence on the stellar structure.

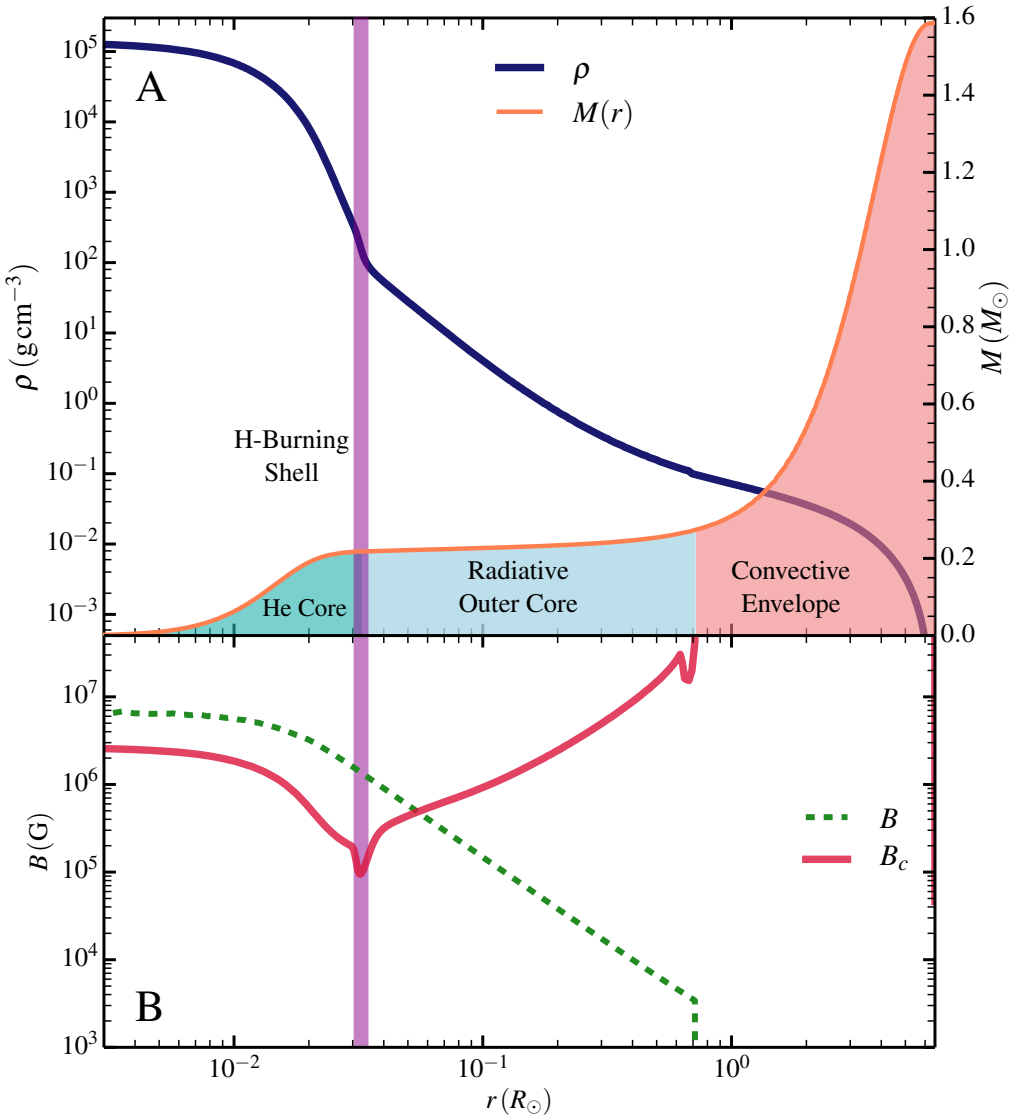

Figure S1: Structure of the $M = 1.6\,M_\odot$ stellar model shown in Fig. 3. (**A**) At this stage of evolution, the star has a $\sim 0.2\,M_\odot$ helium core, surrounded by a $\sim 0.1\,M_\odot$ radiative outer core. The vertical purple band shows the location of the hydrogen-burning shell. The bulk of the mass and radial extent of the star is comprised by the thick convective envelope. (**B**) Core magnetic field. The field strength B is calculated by assuming magnetic flux conservation from a dipole field on the main sequence as described in the supplementary material. We also plot the critical field B_c from Eqn. 3 as in Fig. 3. Because $B > B_c$ in the core of this stellar model, the magnetic greenhouse effect may occur.

S1.2 Mode Visibility

Here we estimate the visibility of modes suppressed via the magnetic greenhouse effect. To do this, we consider the energy balance between driving and damping of a mode. Each mode receives a stochastic energy input $\dot{E}_{\rm in}$ (*10*). At its time-averaged equilibrium amplitude, the energy input and damping rates of the mode are equal, such that

$$\dot{E}_{\rm in} = \dot{E}_{\rm out} = E_\alpha \gamma_\alpha \,, \tag{S3}$$

where E_α is the energy contained in the mode and γ_α is its damping rate.

Modes suppressed via the magnetic greenhouse effect have an extra source of damping determined by the rate at which energy leaks through the evanescent region separating the acoustic cavity from the g mode cavity. For suppressed modes, we assume that any mode energy which leaks into the g mode cavity is completely lost via the magnetic greenhouse effect. Similar calculations have been employed for more evolved red giants where waves entering the core are damped by radiative diffusion (*29–31*). Given some mode energy contained within the acoustic cavity, $E_{\rm ac}$, the rate at which mode energy leaks into the core is

$$\dot{E}_{\rm leak} = \frac{E_{\rm ac}}{t_{\rm leak}}, \tag{S4}$$

where $t_{\rm leak}$ is the time scale on which mode energy leaks into the core. As explained in the text, the energy leakage time scale is

$$t_{\rm leak} = \frac{2t_{\rm cross}}{T^2} \,, \tag{S5}$$

where the transmission coefficient T is

$$T = \exp\left[\int_{r_1}^{r_2} ik_r dr\right]. \tag{S6}$$

The value of T is approximately the fractional decrease in wave amplitude across the evanescent region, whereas T^2 is the fractional decrease in wave energy. In the WKB approximation, the

value of the radial wavenumber k_r within the evanescent region is

$$k_r^2 = \frac{\left(L_\ell^2 - \omega^2\right)\left(N^2 - \omega^2\right)}{v_s^2 \omega^2} \,. \tag{S7}$$

Deep within an evanescent region where $N^2 \ll \omega \ll L_\ell^2$, Eqn. S7 evaluates to $k_r \sim i\sqrt{\ell(\ell+1)}/r$, and Eqn. S6 yields the expression for T in Eqn. 1. The wave crossing time for acoustic waves is

$$t_{\rm cross} = \int_{r_2}^{R} \frac{dr}{v_s} \,. \tag{S8}$$

A suppressed mode is also damped by the same mechanisms as a normal mode. In the case of envelope modes for stars low on the RGB, this damping is created by convective motions near the surface of the star (*10, 32*). The equilibrium energy of the suppressed mode is

$$\dot{E}_{\rm in} = \dot{E}_{\rm out} = E_{\rm ac}\left[\gamma_{\rm ac} + \frac{T^2}{2t_{\rm cross}}\right], \tag{S9}$$

where $\gamma_{\rm ac}$ is the damping rate due to convective motions in the acoustic cavity.

Now, we assume that the suppression mechanism is localized to the core and that the energy input $\dot{E}_{\rm in}$ is unaltered. Then we can set Eqns. S3 and S9 equal to each other to find

$$E_\alpha \gamma_\alpha = E_{\rm ac}\left[\gamma_{\rm ac} + \frac{T^2}{2t_{\rm cross}}\right] . \tag{S10}$$

The damping of a normal mode is localized to the acoustic cavity, so its energy loss rate can be written

$$E_\alpha \gamma_\alpha \simeq E_{\alpha,{\rm ac}} \gamma_{\rm ac} \,, \tag{S11}$$

where $E_{\alpha,{\rm ac}}$ is the mode energy contained in the acoustic cavity. Inserting this into Eqn. S10, we have

$$E_{\alpha,{\rm ac}} \gamma_{\rm ac} = E_{\rm ac}\left[\gamma_{\rm ac} + \frac{T^2}{2t_{\rm cross}}\right] . \tag{S12}$$

The energy of a mode within the envelope is proportional to its surface amplitude squared, hence, the visibility of a mode scales as $V_\alpha^2 \propto E_{\alpha,{\rm ac}}$. Then the ratio of the visibility of the

suppressed mode to that of the normal mode is

$$\frac{V_{\rm sup}^2}{V_{\rm norm}^2} = \frac{E_{\rm ac}}{E_{\alpha,{\rm ac}}} \,. \tag{S13}$$

Then Eqn. S12 leads to

$$\frac{V_{\rm sup}^2}{V_{\rm norm}^2} = \frac{\gamma_{\rm ac}}{\gamma_{\rm ac} + T^2/(2t_{\rm cross})} \,. \tag{S14}$$

Using the fact that the large frequency separation is $\Delta\nu \simeq (2t_{\rm cross})^{-1}$ (*13*) and defining $\tau = \gamma_{\rm ac}^{-1}$, we have our final result:

$$\frac{V_{\rm sup}^2}{V_{\rm norm}^2} = \left[1 + \Delta\nu\tau T^2\right]^{-1} . \tag{S15}$$

The damping time τ is the lifetime of wave energy located in the acoustic cavity. It is not equal to the lifetime of a normal dipole mode, because much of the dipole mode energy resides within the core. Instead, τ is approximately equal to the lifetime of a radial mode, because all of its energy is in the acoustic cavity. Thus, τ can be equated with observed/theoretical lifetimes of radial modes.

We emphasize that the magnetic greenhouse mechanism that operates in depressed dipole oscillators is not directly related to the suppression of solar-like oscillations in stars exhibiting surface magnetic activity (*33–35*). In the latter case, the depression likely arises from magnetic effects in the convective envelope quenching the amplitudes of all oscillation modes, not just the dipole modes.

S1.3 Wave Leakage Time

The wave leakage time scale $t_{\rm leak}$ on which wave energy tunnels from the acoustic cavity into the stellar core can be estimated from Eqn. S5, with the value of T calculated from the first part of Eqn. S6, or approximated from Eqn. 1.

To compute a more precise estimate, we solve the forced adiabatic linearized hydrodynamic (non-magnetic) wave equations for our stellar models (using the Cowling approximation), as-

suming all wave energy that tunnels into the outer core is lost within the inner core. To do this, we place the inner boundary of our computational grid at a radius $r/R = 0.01$, which is always within the stably stratified regions of our red giant models. We then impose a radiative inner boundary condition (*36*). On the outer boundary, we impose a forcing/normalization condition on the real part of the wave displacement vector $\boldsymbol{\xi}$, i.e., we set $\mathrm{Re}\big(\xi_r\big) = 1$, where ξ_r is the radial component of the displacement vector. For the imaginary component, we adopt the standard reflective outer boundary condition, $\mathrm{Im}\big(\delta P\big) = \rho g \mathrm{Im}\big(\xi_r\big)$, where δP is the Eulerian pressure perturbation, ρ is the density, and g is the gravitational acceleration. Physically, this scenario represents the forcing of the stellar surface at a given angular frequency ω, and the eventual leakage of the wave energy into the core of the star.

After solving the wave equations, we compute the leakage time of the wave energy contained within the acoustic cavity at radii $r_2 < r < R$. The wave energy contained within the acoustic cavity is simply

$$E_{\mathrm{ac}} = \int_{r_2}^{R} dr\, \rho r^2 \omega^2 \left(|\xi_r|^2 + \ell(\ell+1)|\xi_\perp|^2 \right), \tag{S16}$$

where $\xi_\perp$ is the horizontal component of the wave displacement vector. The rate at which energy leaks through the inner boundary is

$$\dot{E}_{\mathrm{leak}} = \rho r^3 \omega^3 \Big[\mathrm{Re}\big(\xi_\perp\big)\mathrm{Im}\big(\xi_r\big) - \mathrm{Re}\big(\xi_r\big)\mathrm{Im}\big(\xi_\perp\big) \Big], \tag{S17}$$

evaluated at the inner boundary of the grid. The wave energy leakage time is then

$$t_{\mathrm{leak}} = \frac{E_{\mathrm{ac}}}{\dot{E}_{\mathrm{leak}}}\,. \tag{S18}$$

We have calculated the leakage timescales for waves with frequencies near $\omega_{\mathrm{max}} = 2\pi\nu_{\mathrm{max}}$ for stellar models on the RGB. For this computational technique, the energy E_{ac} contained within the acoustic cavity peaks at the p mode frequencies of the stellar model. The energy loss rate

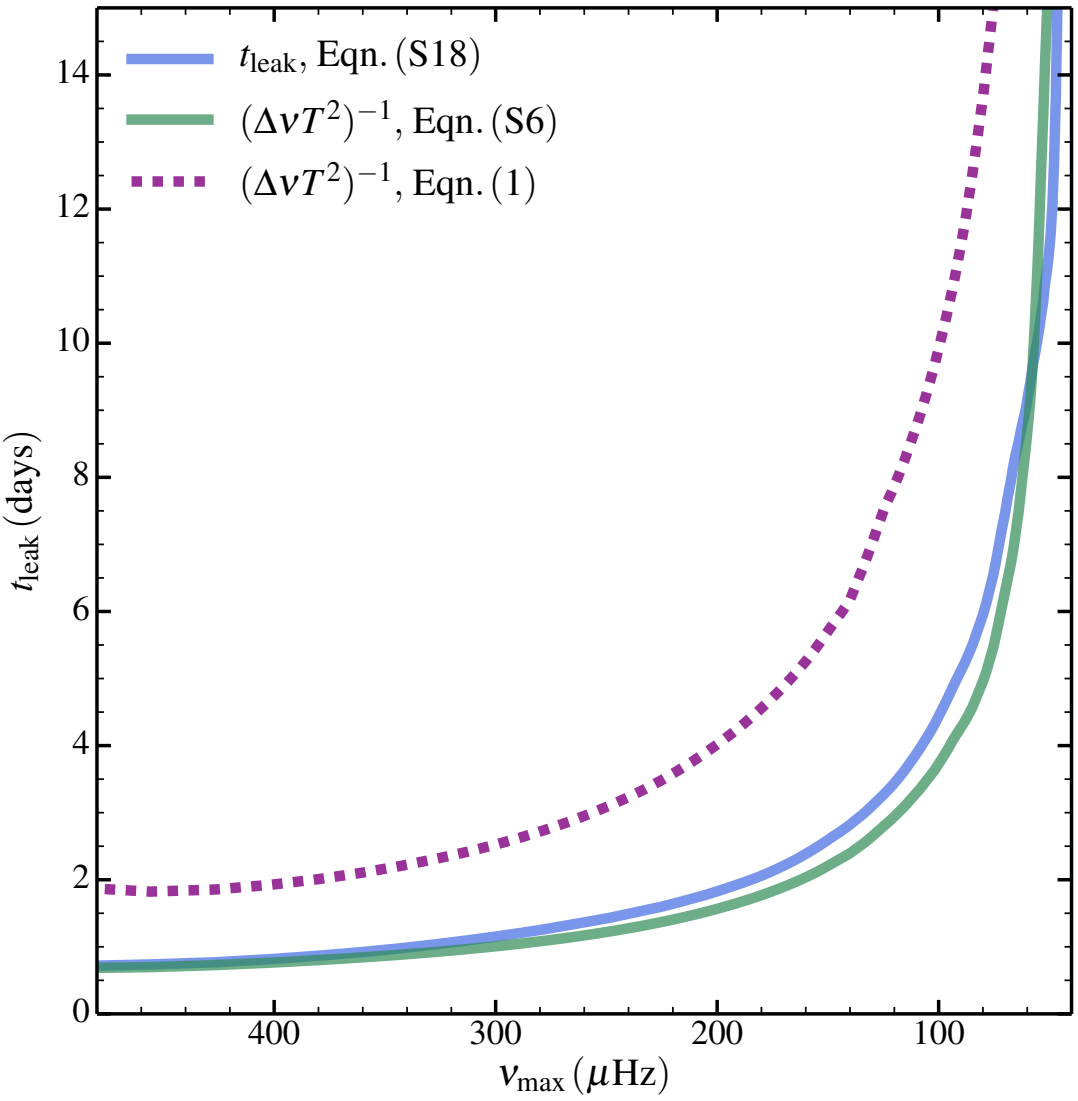

Figure S2: Wave leakage time scale as a function of $\nu_{\rm max}$ for a $1.6\,M_\odot$ stellar model. The leakage timescale has been calculated by solving the linearized wave equations (Eqn. S18), and by approximating it using Eqn. S5, evaluating the transmission coefficient T via Eqn. 1 or S6.

$\dot{E}_{\rm leak}$ also peaks at the mode frequencies, so that the value of $t_{\rm leak}$ is essentially independent of ω.

Fig. S2 shows the exact value of $t_{\rm leak}$ calculated from Eqn. S18, and $t_{\rm leak}$ approximated from Eqn. S5, with T calculated via Eqn.s 1 and S6. Clearly, evaluating $t_{\rm leak}$ via Eqn. S5 with

T calculated from Eqn. S6 is a very good approximation, accurate to within $\sim 10\%$ for our stellar models. However, using the approximation of Eqn. 1 is not very accurate, and generally produces a value of $t_{\rm leak}$ too large by a factor of ~ 2. We conclude that we may accurately estimate mode visibilities using Eqn. 2, so long as the value of T is calculated with an integral over the evanescent region as in Eqn. S6. The approximation of T in Eqn. 1 should not be used for visibility calculations, although it is still useful because it demonstrates the scaling of T with wave angular degree ℓ and the size of the evanescent region.

S1.4 Magneto-Gravity Waves

The properties of magnetohydrodynamic waves in red giant cores can be understood using a local (WKB) analysis for high wavenumbers $\mathbf{k}$, in which $kr \gg 1$ and $kH \gg 1$ (where H is a pressure scale height). We show below the WKB limit is a good approximation in our stellar models. In what follows, we shall also use the adiabatic, anelastic, and ideal MHD approximations, which are all valid for the magneto-gravity waves we consider in red giant cores.

Using the approximations above, the dispersion relation for MHD waves is (*37*)

$$\left(\omega^2 - \omega_A^2\right)\left(\omega^2 - \frac{k_\perp^2}{k^2}N^2 - \omega_A^2\right) = 0. \tag{S19}$$

Here, ω is the angular frequency of the wave, $k_\perp = \sqrt{l(l+1)}/r$ is the horizontal wavenumber, N is the Brunt-Väisälä (buoyancy) frequency, and the Alfvén frequency is

$$\omega_A^2 = \frac{\left(\mathbf{B}\cdot\mathbf{k}\right)^2}{4\pi\rho}, \tag{S20}$$

where $\mathbf{B}$ is the magnetic field and ρ is the density. The Alfvén frequency can also be expressed as

$$\omega_A^2 = v_A^2 k^2 \mu^2, \tag{S21}$$

where v_A is the Alfvén speed,

$$v_A^2 = \frac{B^2}{4\pi\rho}\,. \tag{S22}$$

and $\mu = \cos\theta$ is the angle between the magnetic field and wave vector.

Eqn. S19 has two classes of solutions corresponding to each term in parentheses: Alfvén waves and magneto-gravity waves. Alfvén waves satisfy $\omega^2 = \omega_A^2$ and have wavenumber

$$k^2 = \frac{\omega^2}{\mu^2 v_A^2}. \tag{S23}$$

Alfvén waves have fluid velocity perpendicular to the field lines and group velocity $v_g = v_A$ parallel to magnetic field lines.

Magneto-gravity waves have $\omega^2 = k_\perp^2 N^2/k^2 + \omega_A^2$. A little algebra demonstrates that their wavenumber is

$$k^2 = \frac{\omega^2}{2v_A^2\mu^2}\left[1 \pm \sqrt{1 - \frac{4\mu^2 v_A^2 N^2 k_\perp^2}{\omega^4}}\right]. \tag{S24}$$

The positive and negative roots correspond to the "slow" and "fast" magneto-gravity waves, respectively. In the limit of vanishing magnetic field or buoyancy ($v_A \to 0$ or $N \to 0$), the slow waves reduce to Alfvén waves,

$$k^2 \simeq \frac{\omega^2}{\mu^2 v_A^2}\,. \tag{S25}$$

The fast waves reduce to gravity waves,

$$k^2 \simeq \frac{N^2 k_\perp^2}{\omega^2}\,. \tag{S26}$$

Gravity waves have fluid velocity nearly perpendicular to the stratification (i.e., nearly horizontal). Their group velocity is primarily horizontal, with

$$v_{g,\perp} = \frac{\omega}{k_\perp}\,, \tag{S27}$$

but with a small radial component of

$$v_{g,r} = \frac{\omega^2}{N k_\perp}\,. \tag{S28}$$

In the limit of very strong magnetic field or stratification (such that the second term in the square root of Eqn. S24 dominates), the wavenumber obtains a large imaginary component. Therefore, magneto-gravity waves become evanescent in regions of very strong magnetic field. Low frequency waves approaching regions of high field strength can reflect off the stiff field lines, similar to low frequency fluid waves reflecting off a solid boundary. The evanescent skin depth is small, with $H_{\rm ev} \sim \sqrt{v_A/(Nk_\perp)} \ll H$ when the second term in the square root of Eqn. S24 dominates.

The transition from propagating to evanescent magneto-gravity waves occurs when

$$2\mu v_A = \frac{\omega^2}{Nk_\perp}\,, \tag{S29}$$

i.e., when

$$v_{A,r} \sim v_{g,r}\,. \tag{S30}$$

Here, we have used $\mu v_A \sim v_{A,r}$ because $k_r \gg k_\perp$ for gravity waves in the WKB limit, and therefore $\mathbf{B}\cdot\mathbf{k} \approx B_r k_r$, unless the field is almost completely horizontal. Hence, the *radial* component of the field typically dominates the interaction between the magnetic field and gravity waves. The physical reason for this is that the large horizontal motions and vertical wavenumbers of gravity waves generate large magnetic tension restoring forces by bending radial magnetic field lines.

Fig. S3 shows wave speeds and wavenumbers corresponding to the propagation diagram in Fig. 3. We note that the Alfvén speed is always much less than the sound speed, i.e., the magnetic pressure is much smaller than the gas pressure and the magnetic field has a negligible effect on the background stellar structure. We also note that both Alfvén and magneto-gravity waves always have $k \gg 1/H$ and $k \gg 1/r$ in the inner core of our RGB models. Therefore, the WKB analysis used above is justified.

Several previous works (e.g., (*38*) and references therein) have examined the propagation of

magneto-gravity waves in stellar interiors, focusing primarily on the solar tachocline. However, nearly all of these works have considered a purely toroidal (horizontal) magnetic field configuration, because they were motivated by the strong toroidal field thought to exist due to the shear flows in the solar tachocline. Horizontal fields must be stronger by a factor $k_r/k_\perp \sim N/\omega \gg 1$ in order to strongly affect gravity waves. Consequently, these works did not examine the extremely important effect of radial magnetic fields on gravity wave dynamics.

Finally, many papers (such as (*39*) and references therein) have examined the effect of magnetic fields on the acoustic oscillations of rapidly oscillating Ap stars. In this case, the magnetic field strongly affects the acoustic waves only near the surface of the star where the magnetic pressure becomes comparable to the gas pressure. These authors reach similar conclusions to those discussed below: some wave energy can be lost by transmission into Alfvén waves, and the geometry of the magnetic field is important. However, the oscillation modes in these stars indicates that observable modes can still exist in the presence of strong magnetic fields, and future studies should further examine possible connections between the physics of oscillating Ap stars and red giants with magnetic cores.

S1.5 Reflection/Transmission

We define the magneto-gravity radius, $r_{\rm MG}$, as the radius where $\omega = \omega_{\rm MG}$. At this location, magneto-gravity waves become evanescent and can no longer propagate inward. An incoming wave must either reflect or propagate inward as a pure Alfvén wave.

Incoming $\ell = 1$ magneto-gravity waves can transmit energy into a continuous spectrum (*40, 41*) of Alfvén waves with a broad spectrum of ℓ values (*42*). Reflected waves will also transfer energy to high ℓ waves (for reasons below), and because the location of $r_{\rm MG}$ is a function of latitude since the magnetic field cannot be spherically symmetric. Even in the simplest case of a purely dipolar magnetic field, any resulting oscillation modes will contain a broad spectrum

of ℓ (*43, 44*). In reality, the field will likely have a complex geometry containing both poloidal and toroidal components (*45–47*), and dipole waves will inevitably scatter into higher ℓ waves in the presence of a strong magnetic field.

Wave reflection or transmission at $r_{\rm MG}$ is analogous to the propagation of light between materials of differing refractive indices. In the present case, magneto-gravity waves will likely be reflected due to the high effective refractive index at $r_{\rm MG}$ due to the differing speeds of magneto-gravity and Alfvén waves. Just above $r_{\rm MG}$, the group velocity of the incoming magneto-gravity waves is primarily horizontal and is approximately

$$\mathbf{v}_g \sim \left[\frac{\omega}{k_\perp}\hat{\mathbf{n}}_\perp - \frac{\omega^2}{Nk_\perp}\hat{\mathbf{r}}\right] \sim \left[\frac{\omega}{k_\perp}\hat{\mathbf{n}}_\perp - v_{A,r}\hat{\mathbf{r}}\right]. \tag{S31}$$

Below $r_{\rm MG}$, the group velocity of Alfvén waves is $v_A\hat{\mathbf{B}}$, in the direction of the magnetic field. Thus, although the radial group velocity of the incoming magneto-gravity waves is comparable to that of Alfvén waves, their horizontal group velocity is much larger than the Alfvén velocity. Except in the case of nearly horizontal fields, coupling to Alfvén waves requires a large change in both direction and magnitude of the group velocity. The same is true for the phase velocity. This may cause most of the gravity wave energy to reflect at $r_{\rm MG}$ rather than being transmitted into Alfvén waves.

In the solar atmosphere, an analogous process occurs where magneto-acoustic-gravity waves become magnetically dominated as they propagate upward. In general, the reflection or transmission of the wave depends on the geometry of the magnetic field (*48*). Mostly radial fields tend to reflect waves downward at the effective value of $r_{\rm MG}$ in the solar atmosphere (*49, 50*). Moreover, the waves are reflected onto the slow branch, i.e., they transition into Alfvén waves as they propagate downward. The same process may occur in stellar interiors: ingoing waves will mostly reflect at $r_{\rm MG}$ and will then transition into Alfvén waves as they propagate back outward. Sufficiently horizontal fields will allow more wave transmission into Alfvén waves in

the core, however, stronger fields are required in this case.

The reflected waves will dissipate much faster than the incident dipole waves, preventing them from ever tunneling back to the surface. Waves reflected back onto the fast branch will have higher ℓ, shorter wavelengths, and will damp out more quickly than dipole waves. Waves reflected onto the slow branch have wavenumbers orders of magnitude larger than the fast branch of magneto-gravity waves (see Fig. S3) as they propagate outward into weakly magnetized regions. Therefore, any wave energy reflected into slow magneto-gravity waves will be quickly dissipated via radiative diffusion.

For perfect wave trapping in the core, purely dipole modes only exist in the envelope, with part of their energy leaking into the core as running magneto-gravity waves. If some wave energy does escape the core, it may leave a signature in the form of mixed magneto-gravity acoustic modes, or by producing magnetic mode splitting, which could be used to constrain the internal magnetic field geometry.

S1.6 Ray Tracing

Additional understanding of magneto-gravity waves can be gained using a ray tracing technique. This process allows us to explicitly follow the time evolution of a wave as it propagates into a region of increasing magnetic field. We follow the basic technique outlined in (*51*). In the case of magneto-gravity waves in the WKB limit, the Hamiltonian describing their equations of motion is

$$H = \omega = \sqrt{\frac{{\mathbf{k}_\perp}^2 N^2}{\mathbf{k}^2} + (\mathbf{k} \cdot \mathbf{v_A})^2}\,. \tag{S32}$$

In reality, the Hamiltonian contains additional terms that allow for the existence of pure Alfvén waves, although we neglect this subtlety here.

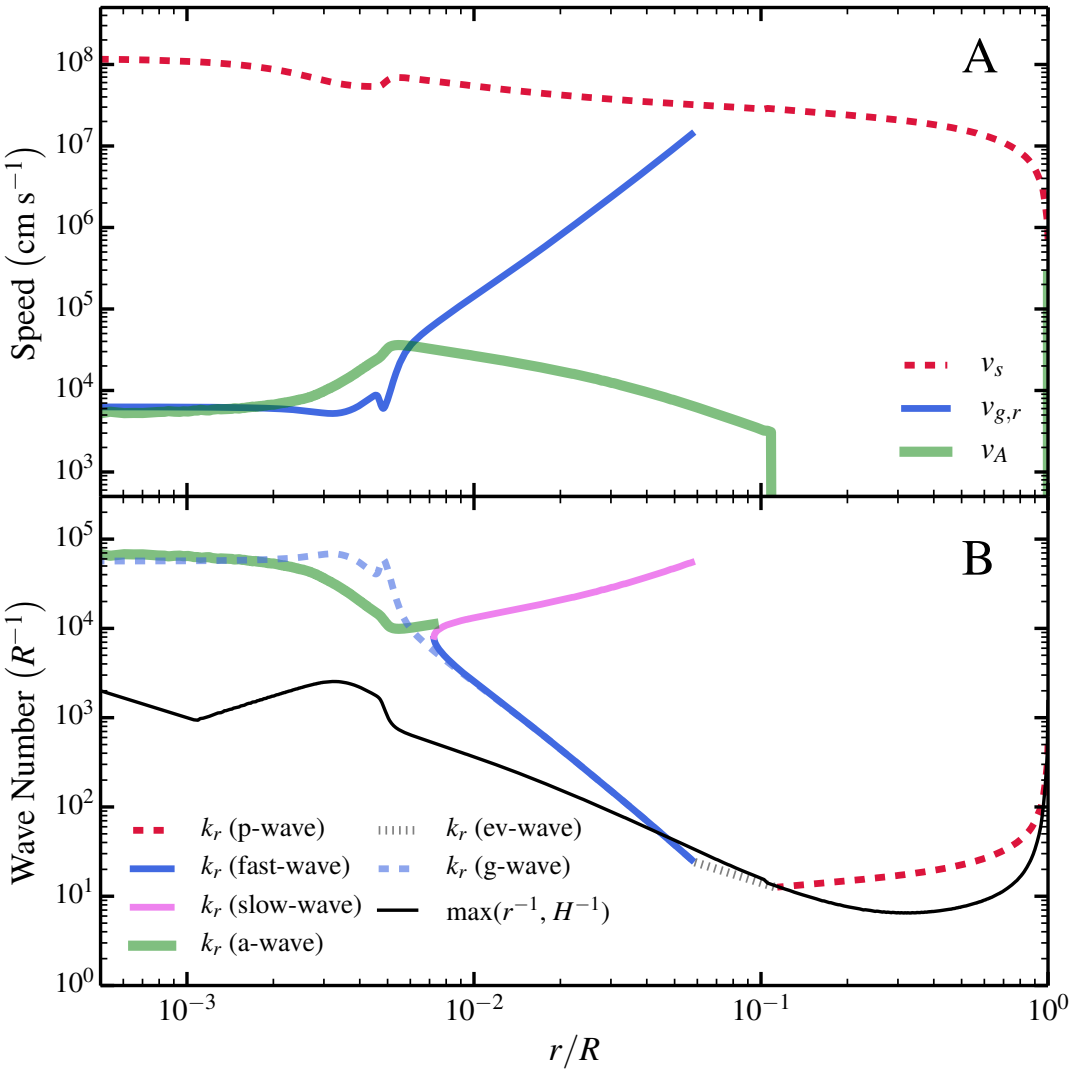

Figure S3: Wave properties of the stellar model shown in Figs. 3 and S1. (**A**) The sound speed, v_s, gravity wave radial group velocity, $v_{g,r}$ (for $\omega = 2\pi\nu_{\max}$), and Alfvén speed, v_A. Waves travel at a group velocity of v_s, $v_{g,r}$, and v_A for acoustic, gravity, and Alfvén waves, respectively. **(B)** Radial wave number, k_r, for a wave with $\omega = 2\pi\nu_{\max}$, as a function of radius. We have plotted the wavenumbers of acoustic waves (p-waves), fast magneto-gravity waves (fast-waves), slow magneto-gravity waves (slow-waves), Alfvén waves (a-waves), and the evanescent part of the wave (ev-wave). The dashed blue line shows the wavenumber for gravity waves (g-waves) in the absence of a magnetic field. The solid black line shows the maximum of r^{-1} or H^{-1} (where H is a pressure scale height).

The equations of motion corresponding to the Hamiltonian of Eqn. S32 are

$$\frac{d\mathbf{x}}{dt} = \frac{\partial H}{\partial \mathbf{k}} = \frac{N^2}{\omega k}\left[\left(1 - \frac{k_\perp^2}{k^2}\right)\frac{\mathbf{k}_\perp}{k} - \frac{k_\perp^2}{k^2}\frac{k_r \hat{\mathbf{r}}}{k}\right] + \frac{\omega_A}{\omega}\mathbf{v_A}\,, \tag{S33}$$

where $\omega_A = (\mathbf{k}\cdot\mathbf{v_A})$, and

$$\frac{d\mathbf{k}}{dt} = -\frac{\partial H}{\partial \mathbf{x}} = -\frac{N}{\omega}\frac{k_\perp^2}{k^2}\nabla N - \frac{\omega_A}{\omega}\nabla\big(\mathbf{k}\cdot\mathbf{v_A}\big)\,. \tag{S34}$$

Eqn. S33 describes the group velocity of the wave, while Eqn. S34 describes the evolution of its wave vector, which is related to the momentum of the wave. Note that in the absence of a magnetic field in a spherical star, only the radial component of the wave vector changes, and the horizontal component is conserved. This is not surprising because the Hamiltonian is spherically symmetric and thus angular momentum (and hence angular wave vector) is conserved.

However, in the presence of a magnetic field, the last term of Eqn. S34 breaks the spherical symmetry. Except in the unphysical case of a purely radial field or a constant field, this term is non-zero, and therefore the angular component of the wave vector must change. At the radius $r_{\rm MG}$ where $v_A \sim \omega^2/(Nk_\perp)$, each term in Eqn. S34 is the same order of magnitude, assuming $|\nabla B|/B \sim 1/r$. Therefore, the rate of change in horizontal wavenumber is comparable to the rate of change in radial wavenumber at field strengths near B_c. Upon wave reflection or conversion into Alfvén waves, the radial wavenumber will generally change by order unity, i.e., the change in radial wavenumber is $|\Delta k_r| \sim |k_r|$. We therefore expect a correspondingly large change in $k_\perp$, such that $|\Delta k_\perp| \sim |k_r|$. Hence, dipole waves will generally obtain high multipole moments when they propagate through strongly magnetized regions of the star.

S1.7 Joule Damping

A gravity wave propagating through a magnetized fluid induces currents which dissipate in a non-perfectly conducting fluid, causing the wave to damp. For gravity waves in the WKB limit which are not strongly altered by magnetic tension forces, the perturbed radial magnetic

field is $\delta B \approx \xi_\perp k_r B$, where $\xi_\perp$ is the horizontal wave displacement. The perturbed current density is $\delta J \approx c k_r \delta B/(4\pi)$, where c is the speed of light. The volumetric energy dissipation rate is $\dot{\varepsilon} \approx (\delta J)^2/\sigma$, where σ is the electrical conductivity. The gravity wave energy density is $\varepsilon \approx \rho\omega^2\xi_\perp^2$, so the local damping rate is

$$\Gamma_B = \frac{\dot{\varepsilon}}{\varepsilon} \approx \frac{\eta B^2 k_r^4}{(4\pi)^2 \rho\omega^2}\,, \tag{S35}$$

where $\eta = c^2/\sigma$ is the magnetic diffusivity.

The Joule damping rate of Eqn. S35 can be compared with the damping rate from radiative diffusion (in the absence of composition gradients), $\Gamma_r = k_r^2\kappa$, where κ is the thermal diffusivity. The ratio of Joule damping to thermal damping is

$$\frac{\Gamma_B}{\Gamma_r} = \frac{\eta}{\kappa}\frac{B^2 k_r^2}{(4\pi)^2\rho\omega^2} = \frac{\eta}{\kappa}\frac{l(l+1)B^2N^2}{(4\pi)^2\rho r^2\omega^4}\,, \tag{S36}$$

and the second equality follows from using the gravity wave dispersion relation. The maximum magnetic field possible before Lorentz forces strongly alter gravity waves is B_c (Eqn. 3), and putting this value into Eqn. S36 we find

$$\frac{\Gamma_B}{\Gamma_r} = \frac{1}{16\pi}\frac{\eta}{\kappa}\,. \tag{S37}$$

Therefore, for gravity waves, Joule damping cannot exceed thermal damping unless the magnetic diffusivity is significantly larger than the thermal diffusivity. In stellar interiors (and our RGB models), the magnetic diffusivity is typically orders of magnitude smaller than the thermal diffusivity. Therefore Joule damping can safely be ignored. We note that the same result occurs if we use the Alfvén wave dispersion relation in Eqn. S36, so Joule damping is also unimportant for Alfvén waves.

S1.8 Measurements and Uncertainties

Most of the observational data shown in Fig. 2 were obtained from (*6*). The additional stars KIC 8561221 and KIC 9073950 were analyzed using the same methods as (*6*). This analysis pro-

Star	$\nu_{\rm max}$ (μHz)	$\Delta\nu$ (μHz)	$T_{\rm eff}$ (K)	M ($M_\odot$)	B_r (G)
KIC8561221	490 ± 24	29.88 ± 0.80	5245 ± 60	1.5 ± 0.1	$1.5^{+2.4}_{-0.4} \times 10^7$
KIC9073950	291 ± 25	20.99 ± 0.64	5087 ± 200	1.2 ± 0.2	$> 1.3 \times 10^6$

Table S1: Properties of stars shown in Fig. 4.

vided measured values of dipole mode visibility V^2, $\nu_{\rm max}$, $\Delta\nu$, and their associated uncertainties. For KIC9073950, we used the updated KIC $T_{\rm eff}$ (*52*) to calculate mass and its uncertainty from scaling relations. For KIC8561221, mass and uncertainties were obtained from (*8*). To calculate values of B_c for KIC8561221 and KIC9073950, we interpolated in $\log B_c$ between the tracks shown in Fig. 4, using the measured stellar masses. The uncertainty in B_c was obtained by performing the same interpolation on the upper and lower bounds of the stellar mass.

S1.9 ε Ophiuchi

The red giant ε Ophiuchi, extensively observed with ground-based instruments (*53*) and with the *MOST* satellite (*54*), may also exhibit depressed dipole modes. Its temperature of $\approx 4900\,{\rm K}$, inferred mass of $1.85 \pm 0.05\,M_\odot$ and interferometricly measured radius of $10.39 \pm 0.07\,R_\odot$ (*55*) yield $\nu_{\rm max} \approx 57\,\mu{\rm Hz}$ and $\Delta\nu \approx 5.5\,\mu{\rm Hz}$. This is consistent with the interpretation (*53–55*) that many of the peaks in its *M*OST power spectrum belong to a series of radial oscillation modes. However, we agree with (*56*) that the most likely explanation for the power spectrum is that it is created by a combination of both radial and non-radial modes.

We speculate that the low amplitude and missing dipole modes can be explained if ε Ophiuchi is a depressed dipole mode star. At this stage of evolution, we expect the normalized depressed dipole mode power V^2 and lifetime τ to be roughly half their normal values. The measured lifetimes of $\tau \sim 12\,{\rm days}$ (*56*) are dominated by radial and envelope-dominated quadrupole modes, and are consistent with the usual lifetimes of these modes in red giants

at this stage of evolution. A more robust conclusion would require a comparison of measured radial mode line widths to dipole mode line widths, and our scenario would predict that the dipole modes should have lifetimes of $\tau \sim 6\,\mathrm{days}$. We suspect that overlapping radial and quadrupole modes may help explain the large line widths found by (*54*), who considered the peaks to be produced solely by radial modes.

S1.10 MESA Inlist

Here is the inlist used to calculate the stellar evolution models discussed in the paper.

```
&star_job
      change_lnPgas_flag = .true.
      new_lnPgas_flag = .true.
      pgstar_flag = .true.
/ ! end of star_job namelist


&controls
      !----------------------------------------  MAIN
      initial_mass = 1.3
      initial_z = 0.02
      use_Type2_opacities = .true.
      Zbase = 0.02
      !----------------------------------------  WIND
      RGB_wind_scheme = 'Reimers'
      Reimers_wind_eta = 0.5d0
      RGB_to_AGB_wind_switch = 1d-4
      AGB_wind_scheme = 'Blocker'
```

```
      Blocker_wind_eta = 5d0  ! 0.7d0
      !-----------------------------------  OVERSHOOTING
      overshoot_f_below_nonburn = 0.018
      overshoot_f_above_burn_h = 0.018
      overshoot_f_above_burn_he = 0.018
      !-----------------------------------  MISC
      photostep = 100
      profile_interval = 100
      max_num_profile_models = 100
      history_interval = 1
      terminal_cnt = 10
      write_header_frequency = 10
      max_number_backups = 50
      max_number_retries = 100
      max_timestep = 3.15d14  ! in seconds
      !-----------------------------------  MESH
      mesh_delta_coeff = 0.8
      !-----------------------------------  STOP WHEN
      xa_central_lower_limit_species(1) = 'he4'
      xa_central_lower_limit(1) = 0.05
/ ! end of controls namelist
&pgstar
/ ! end of pgstar namelist
```

REFERENCES AND NOTES

1. T. R. Bedding, *Solar-like Oscillations: An Observational Perspective* (Cambridge Univ. Press, Cambridge, 2014).

2. P. G. Beck, T. R. Bedding, B. Mosser, D. Stello, R. A. Garcia, T. Kallinger, S. Hekker, Y. Elsworth, S. Frandsen, F. Carrier, J. De Ridder, C. Aerts, T. R. White, D. Huber, M. A. Dupret, J. Montalbán, A. Miglio, A. Noels, W. J. Chaplin, H. Kjeldsen, J. Christensen-Dalsgaard, R. L. Gilliland, T. M. Brown, S. D. Kawaler, S. Mathur, J. M. Jenkins, Kepler detected gravity-mode period spacings in a red giant star. *Science* **332**, 205 (2011). Medline

3. T. R. Bedding, B. Mosser, D. Huber, J. Montalbán, P. Beck, J. Christensen-Dalsgaard, Y. P. Elsworth, R. A. García, A. Miglio, D. Stello, T. R. White, J. De Ridder, S. Hekker, C. Aerts, C. Barban, K. Belkacem, A. M. Broomhall, T. M. Brown, D. L. Buzasi, F. Carrier, W. J. Chaplin, M. P. Di Mauro, M. A. Dupret, S. Frandsen, R. L. Gilliland, M. J. Goupil, J. M. Jenkins, T. Kallinger, S. Kawaler, H. Kjeldsen, S. Mathur, A. Noels, V. S. Aguirre, P. Ventura, Gravity modes as a way to distinguish between hydrogen- and helium-burning red giant stars. *Nature* **471**, 608–611 (2011). Medline doi:10.1038/nature09935

4. B. Mosser, O. Benomar, K. Belkacem, M. J. Goupil, N. Lagarde, E. Michel, Y. Lebreton, D. Stello, M. Vrard, C. Barban, T. R. Bedding, S. Deheuvels, W. J. Chaplin, J. De Ridder, Y. Elsworth, J. Montalban, A. Noels, R. M. Ouazzani, R. Samadi, T. R. White, H. Kjeldsen, Mixed modes in red giants: A window on stellar evolution. *Astron. Astrophys.* **572**, L5 (2014). doi:10.1051/0004-6361/201425039

5. P. G. Beck, J. Montalban, T. Kallinger, J. De Ridder, C. Aerts, R. A. García, S. Hekker, M. A. Dupret, B. Mosser, P. Eggenberger, D. Stello, Y. Elsworth, S. Frandsen, F. Carrier, M. Hillen, M. Gruberbauer, J. Christensen-Dalsgaard, A. Miglio, M. Valentini, T. R. Bedding, H. Kjeldsen, F. R. Girouard, J. R. Hall, K. A. Ibrahim, Fast core rotation in red-giant stars as revealed by gravity-dominated mixed modes. *Nature* **481**, 55–57 (2011). Medline doi:10.1038/nature10612

6. B. Mosser, M. J. Goupil, K. Belkacem, J. P. Marques, P. G. Beck, S. Bloemen, J. De Ridder, C. Barban, S. Deheuvels, Y. Elsworth, S. Hekker, T. Kallinger, R. M. Ouazzani, M. Pinsonneault, R. Samadi, D. Stello, R. A. García, T. C. Klaus, J. Li, S. Mathur, R. L. Morris, Spin down of the core rotation in red giants. *Astron. Astrophys.* **548**, A10 (2012). doi:10.1051/0004-6361/201220106

7. B. Mosser, Y. Elsworth, S. Hekker, D. Huber, T. Kallinger, S. Mathur, K. Belkacem, M. J. Goupil, R. Samadi, C. Barban, T. R. Bedding, W. J. Chaplin, R. A. García, D. Stello, J. De Ridder, C. K. Middour, R. L. Morris, E. V. Quintana, Characterization of the power excess of solar-like oscillations in red giants with *Kepler*. *Astron. Astrophys.* **537**, A30 (2012). doi:10.1051/0004-6361/201117352

8. R. A. García, F. Pérez Hernández, O. Benomar, V. Silva Aguirre, J. Ballot, G. R. Davies, G. Doğan, D. Stello, J. Christensen-Dalsgaard, G. Houdek, F. Lignières, S. Mathur, M. Takata, T. Ceillier, W. J. Chaplin, S. Mathis, B. Mosser, R. M. Ouazzani, M. H. Pinsonneault, D. R. Reese, C. Régulo, D. Salabert, M. J. Thompson, J. L. van Saders, C. Neiner, J. De Ridder, Study of KIC 8561221 observed by *Kepler* : An early red giant

showing depressed dipolar modes. *Astron. Astrophys.* **563**, A84 (2014). doi:10.1051/0004-6361/201322823

9. P. Goldreich, D. A. Keeley, Solar seismology. II - The stochastic excitation of the solar p-modes by turbulent convection. *Astrophys. J.* **212**, 243 (1977). doi:10.1086/155043

10. M.-A. Dupret, K. Belkacem, R. Samadi, J. Montalban, O. Moreira, A. Miglio, M. Godart, P. Ventura, H.-G. Ludwig, A. Grigahcène, M.-J. Goupil, A. Noels, E. Caffau, Theoretical amplitudes and lifetimes of non-radial solar-like oscillations in red giants. *Astron. Astrophys.* **506**, 57–67 (2009). doi:10.1051/0004-6361/200911713

11. O. Benomar, K. Belkacem, T. R. Bedding, D. Stello, M. P. Di Mauro, R. Ventura, B. Mosser, M. J. Goupil, R. Samadi, R. A. Garcia, Asteroseismology of evolved stars with *Kepler*: A new way to constrain stellar interiors using mode inertias. *Astrophys. J.* **781**, L29 (2014). doi:10.1088/2041-8205/781/2/L29

12. See the supplementary materials on *Science* Online.

13. W. J. Chaplin, A. Miglio, Asteroseismology of solar-type and red-giant stars. *Annu. Rev. Astron. Astrophys.* **51**, 353–392 (2013). doi:10.1146/annurev-astro-082812-140938

14. E. Corsaro, D. Stello, D. Huber, T. R. Bedding, A. Bonanno, K. Brogaard, T. Kallinger, O. Benomar, T. R. White, B. Mosser, S. Basu, W. J. Chaplin, J. Christensen-Dalsgaard, Y. P. Elsworth, R. A. García, S. Hekker, H. Kjeldsen, S. Mathur, S. Meibom, J. R. Hall, K. A. Ibrahim, T. C. Klaus, Asteroseismology of the open clusters NGC 6791, NGC 6811, and NGC 6819 from 19 months of *Kepler* photometry. *Astrophys. J.* **757**, 190 (2012). doi:10.1088/0004-637X/757/2/190

15. M. Grosjean, M.-A. Dupret, K. Belkacem, J. Montalban, R. Samadi, B. Mosser, Theoretical power spectra of mixed modes in low-mass red giant stars. *Astron. Astrophys.* **572**, A11 (2014). doi:10.1051/0004-6361/201423827

16. E. Corsaro, J. De Ridder, R. A. García, Bayesian peak bagging analysis of 19 low-mass low-luminosity red giants observed with *Kepler*. *Astron. Astrophys.* **579**, A83 (2015). doi:10.1051/0004-6361/201525895

17. T. R. Bedding, D. Huber, D. Stello, Y. P. Elsworth, S. Hekker, T. Kallinger, S. Mathur, B. Mosser, H. L. Preston, J. Ballot, C. Barban, A. M. Broomhall, D. L. Buzasi, W. J. Chaplin, R. A. García, M. Gruberbauer, S. J. Hale, J. De Ridder, S. Frandsen, W. J. Borucki, T. Brown, J. Christensen-Dalsgaard, R. L. Gilliland, J. M. Jenkins, H. Kjeldsen, D. Koch, K. Belkacem, L. Bildsten, H. Bruntt, T. L. Campante, S. Deheuvels, A. Derekas, M.-A. Dupret, M.-J. Goupil, A. Hatzes, G. Houdek, M. J. Ireland, C. Jiang, C. Karoff, L. L. Kiss, Y. Lebreton, A. Miglio, J. Montalbán, A. Noels, I. W. Roxburgh, V. Sangaralingam, I. R. Stevens, M. D. Suran, N. J. Tarrant, A. Weiss, Solar-like oscillations in low-luminosity red giants: First results from *Kepler*. *Astrophys. J.* **713**, L176–L181 (2010). doi:10.1088/2041-8205/713/2/L176

18. T. M. Brown, R. L. Gilliland, R. W. Noyes, L. W. Ramsey, Detection of possible p-mode oscillations on Procyon. *Astrophys. J.* **368**, 599 (1991). doi:10.1086/169725

19. M. Aurière, G. A. Wade, J. Silvester, F. Lignières, S. Bagnulo, K. Bale, B. Dintrans, J. F. Donati, C. P. Folsom, M. Gruberbauer, A. Hui Bon Hoa, S. Jeffers, N. Johnson, J. D. Landstreet, A. Lèbre, T. Lueftinger, S. Marsden, D. Mouillet, S. Naseri, F. Paletou, P. Petit,

J. Power, F. Rincon, S. Strasser, N. Toqué, Weak magnetic fields in Ap/Bp stars. *Astron. Astrophys.* **475**, 1053–1065 (2007). doi:10.1051/0004-6361:20078189

20. S. Deheuvels, G. Doğan, M. J. Goupil, T. Appourchaux, O. Benomar, H. Bruntt, T. L. Campante, L. Casagrande, T. Ceillier, G. R. Davies, P. De Cat, J. N. Fu, R. A. García, A. Lobel, B. Mosser, D. R. Reese, C. Regulo, J. Schou, T. Stahn, A. O. Thygesen, X. H. Yang, W. J. Chaplin, J. Christensen-Dalsgaard, P. Eggenberger, L. Gizon, S. Mathis, J. Molenda-Żakowicz, M. Pinsonneault, Seismic constraints on the radial dependence of the internal rotation profiles of six *Kepler* subgiants and young red giants. *Astron. Astrophys.* **564**, A27 (2014). doi:10.1051/0004-6361/201322779

21. C. Charbonnel, J.-P. Zahn, Inhibition of thermohaline mixing by a magnetic field in Ap star descendants: Implications for the Galactic evolution of ^{3}He. *Astron. Astrophys.* **476**, L29–L32 (2007). doi:10.1051/0004-6361:20078740

22. J. Ballot, C. Barban, C. V. Veer-Menneret, Visibilities and bolometric corrections for stellar oscillation modes observed by *Kepler*. *Astron. Astrophys.* **531**, A124 (2011). doi:10.1051/0004-6361/201016230

23. B. Paxton, L. Bildsten, A. Dotter, F. Herwig, P. Lesaffre, F. Timmes, MODULES FOR EXPERIMENTS IN STELLAR ASTROPHYSICS (MESA). *Astrophys. J. Suppl. Ser.* **192**, 3 (2011). doi:10.1088/0067-0049/192/1/3

24. B. Paxton, M. Cantiello, P. Arras, L. Bildsten, E. F. Brown, A. Dotter, C. Mankovich, M. H. Montgomery, D. Stello, F. X. Timmes, R. Townsend, Modules For Experiments in Stellar Astrophysics (MESA): Planets, oscillations, rotation, and massive stars. *Astrophys. J. Suppl. Ser.* **208**, 4 (2013). doi:10.1088/0067-0049/208/1/4

25. M. Asplund, N. Grevesse, A. J. Sauval, *Astron. Soc. Pac. Conf. Ser.* **336**, 25 (2005).

26. C. A. Iglesias, F. J. Rogers, Updated Opal opacities. *Astrophys. J.* **464**, 943 (1996). doi:10.1086/177381

27. F. Herwig, *Astron. Astrophys.* **360**, 952 (2000).

28. N. A. Featherstone, M. K. Browning, A. S. Brun, J. Toomre, Effects of fossil magnetic fields on convective core dynamos in A-type stars. *Astrophys. J.* **705**, 1000–1018 (2009). doi:10.1088/0004-637X/705/1/1000

29. W. Dziembowski, *Acta Astronomica* **27**, 95 (1977).

30. Y. Osaki, *Proc. Astron. Soc. Jap.* **29**, 235 (1977).

31. W. A. Dziembowski, Dipolar modes in luminous red giants. *Astron. Astrophys.* **539**, A83 (2012). doi:10.1051/0004-6361/201117733

32. G. Houdek, N. J. Balmforth, J. Christensen-Dalsgaard, D. O. Gough, *Astron. Astrophys.* **351**, 582 (1999).

33. R. A. García, S. Mathur, D. Salabert, J. Ballot, C. Régulo, T. S. Metcalfe, A. Baglin, CoRoT reveals a magnetic activity cycle in a Sun-like star. *Science* **329**, 1032 (2010). Medline doi:10.1126/science.1191064

34. W. J. Chaplin, T. R. Bedding, A. Bonanno, A.-M. Broomhall, R. A. García, S. Hekker, D. Huber, G. A. Verner, S. Basu, Y. Elsworth, G. Houdek, S. Mathur, B. Mosser, R. New, I.

R. Stevens, T. Appourchaux, C. Karoff, T. S. Metcalfe, J. Molenda-Żakowicz, M. J. P. F. G. Monteiro, M. J. Thompson, J. Christensen-Dalsgaard, R. L. Gilliland, S. D. Kawaler, H. Kjeldsen, J. Ballot, O. Benomar, E. Corsaro, T. L. Campante, P. Gaulme, S. J. Hale, R. Handberg, E. Jarvis, C. Régulo, I. W. Roxburgh, D. Salabert, D. Stello, F. Mullally, J. Li, W. Wohler, Evidence for the impact of stellar activity on the detectability of solar-like oscillations observed by *Kepler*. *Astrophys. J.* **732**, L5 (2011). doi:10.1088/2041-8205/732/1/L5

35. P. Gaulme, J. Jackiewicz, T. Appourchaux, B. Mosser, Surface activity and oscillation amplitudes of red giants in eclipsing binaries. *Astrophys. J.* **785**, 5 (2014). doi:10.1088/0004-637X/785/1/5

36. J. Fuller, D. Lai, *Mon. Not. R. Astron. Soc.* **421**, 426–445 (2012).

37. W. Unno, Y. Osaki, H. Ando, H. Saio, H. Shibahashi, *Nonradial Oscillations of Stars* (Univ. of Tokyo Press, Tokyo, 1989).

38. S. Mathis, N. de Brye, Low-frequency internal waves in magnetized rotating stellar radiation zones. *Astron. Astrophys.* **540**, A37 (2012). doi:10.1051/0004-6361/201118322

39. H. Saio, M. Gruberbauer, W. W. Weiss, J. M. Matthews, T. Ryabchikova, Pulsation models for the roAp star HD 134214. *Mon. Not. R. Astron. Soc.* **420**, 283–290 (2012). doi:10.1111/j.1365-2966.2011.20031.x

40. D. Reese, F. Rincon, M. Rieutord, Oscillations of magnetic stars. *Astron. Astrophys.* **427**, 279–292 (2004). doi:10.1051/0004-6361:20040539

41. Y. Levin, QPOs during magnetar flares are not driven by mechanical normal modes of the crust. *Mon. Not. R. Astron. Soc.* **368**, L35–L38 (2006). doi:10.1111/j.1745-3933.2006.00155.x

42. F. Rincon, M. Rieutord, Oscillations of magnetic stars: I. Axisymmetric shear Alfvén modes of a spherical shell in a dipolar magnetic field. *Astron. Astrophys.* **398**, 663–675 (2003). doi:10.1051/0004-6361:20021671

43. U. Lee, Axisymmetric oscillations of magnetic neutron stars. *Mon. Not. R. Astron. Soc.* **374**, 1015–1029 (2007). doi:10.1111/j.1365-2966.2006.11214.x

44. U. Lee, *Mon. Not. R. Astron. Soc.* **405**, 1444 (2010).

45. J. Braithwaite, H. C. Spruit, A fossil origin for the magnetic field in A stars and white dwarfs. *Nature* **431**, 819–821 (2004). Medline doi:10.1038/nature02934

46. J. Braithwaite, Å. Nordlund, Stable magnetic fields in stellar interiors. *Astron. Astrophys.* **450**, 1077–1095 (2006). doi:10.1051/0004-6361:20041980

47. V. Duez, J. Braithwaite, S. Mathis, On the stability of non-force-free magnetic equilibria in stars. *Astrophys. J.* **724**, L34–L38 (2010). doi:10.1088/2041-8205/724/1/L34

48. Y. D. Zhugzhda, N. S. Dzhalilov, *Astron. Astrophys.* **132**, 52 (1984).

49. M. E. Newington, P. S. Cally, Reflection and conversion of magnetogravity waves in the solar chromosphere: Windows to the upper atmosphere. *Mon. Not. R. Astron. Soc.* **402**, 386–394 (2010). doi:10.1111/j.1365-2966.2009.15884.x

50. M. E. Newington, P. S. Cally, Mode conversion of radiatively damped magnetogravity waves in the solar chromosphere. *Mon. Not. R. Astron. Soc.* **417**, 1162–1169 (2011). doi:10.1111/j.1365-2966.2011.19332.x

51. F. Lignières, B. Georgeot, Asymptotic analysis of high-frequency acoustic modes in rapidly rotating stars. *Astron. Astrophys.* **500**, 1173–1192 (2009). doi:10.1051/0004-6361/200811165

52. D. Huber, V. S. Aguirre, J. M. Matthews, M. H. Pinsonneault, E. Gaidos, R. A. García, S. Hekker, S. Mathur, B. Mosser, G. Torres, F. A. Bastien, S. Basu, T. R. Bedding, W. J. Chaplin, B.-O. Demory, S. W. Fleming, Z. Guo, A. W. Mann, J. F. Rowe, A. M. Serenelli, M. A. Smith, D. Stello, Revised stellar properties of *Kepler* targets for the quarter 1-16 transit detection run. *Astrophys. J. Suppl. Ser.* **211**, 2 (2014). doi:10.1088/0067-0049/211/1/2

53. J. De Ridder, C. Barban, F. Carrier, A. Mazumdar, P. Eggenberger, C. Aerts, S. Deruyter, J. Vanautgaerden, Discovery of solar-like oscillations in the red giant ε Ophiuchi. *Astron. Astrophys.* **448**, 689–695 (2006). *Astron. Astrophys.* **448**, 689 (2006). doi:10.1051/0004-6361:20053331

54. C. Barban, J. M. Matthews, J. De Ridder, F. Baudin, R. Kuschnig, A. Mazumdar, R. Samadi, D. B. Guenther, A. F. J. Moffat, S. M. Rucinski, D. Sasselov, G. A. H. Walker, W. W. Weiss, Detection of solar-like oscillations in the red giant star ε Ophiuchi by MOST spacebased photometry. *Astron. Astrophys.* **468**, 1033–1038 (2007). doi:10.1051/0004-6361:20066716

55. A. Mazumdar, A. Mérand, P. Demarque, P. Kervella, C. Barban, F. Baudin, V. Coudé du Foresto, C. Farrington, P. J. Goldfinger, M.-J. Goupil, E. Josselin, R. Kuschnig, H. A. McAlister, J. Matthews, S. T. Ridgway, J. Sturmann, L. Sturmann, T. A. ten Brummelaar, N. Turner, Asteroseismology and interferometry of the red giant star ε Ophiuchi. *Astron. Astrophys.* **503**, 521–531 (2009). doi:10.1051/0004-6361/200912351

56. T. Kallinger, D. B. Guenther, J. M. Matthews, W. W. Weiss, D. Huber, R. Kuschnig, A. F. J. Moffat, S. M. Rucinski, D. Sasselov, Nonradial *p* -modes in the G9.5 giant ε Ophiuchi? Pulsation model fits to MOST photometry. *Astron. Astrophys.* **478**, 497–505 (2008). doi:10.1051/0004-6361:20078171